Research Article

Siaw Foon Lee*, Jose Fullea García, Seong Shan Yap*, and David Hui

Pitting corrosion induced on high-strength high carbon steel wire in high alkaline deaerated chloride electrolyte

https://doi.org/10.1515/ntrev-2022-0060 received August 11, 2021; accepted January 28, 2022

Abstract: Electrochemical response causing pitting corrosion of high-strength high carbon steel wire in deaerated electrolyte at pH 13.4 due to different chloride ion (Cl⁻) concentrations was investigated using open circuit potential, cyclic potentiodynamic polarization, and anodic potentiostatic application (APA) within the passive zone. Results showed that the higher the Cl⁻ concentration, the more negative the corrosion potential becomes. In the high alkaline pH 13.4 without the presence of free oxygen gas the Cl⁻ concentration could reach up to 1M not showing pitting potential. An inverse relationship between anodic potentials (APs) and Cl⁻ concentrations was found and the rate of corrosion within passive period was almost a constant, not influenced by the Cl⁻ concentrations. Faraday's law failed to predict the mass loss when active pitting corrosion occurred. Green rust and hydrogen gas were observed during active pitting corrosion under APA. Pitting corrosion mechanism in the deaerated high alkaline electrolyte was then proposed. This work deduces that in the deaerated electrolyte at pH 13.4 with the presence of Cl⁻, it is essential to apply the APs within the safety margin on the high-strength high carbon steel wire to avoid active pitting corrosion and hydrogen embrittlement.

Keywords: pitting corrosion, anodic potential, deaerated high alkaline

David Hui: Department of Mechanical Engineering, University of New Orleans, New Orleans, LA 70148, United States of America

1 Introduction

Reinforcing steels embedded in traditional concrete structures, such as bridges and flyovers, are protected from corrosion using either the cathodic protection that needs the use of other metal as an anode in the sacrificial passive system [1,2], or the anodic protection that applies anodic current to the reinforcing steel [3]. With the increase in daily load, wind load, and earthquake, high-strength high carbon steel wire (HSHCsw) has started to be widely incorporated in the concrete structure to increase its durability.

Until now, the studies on HSHCsw are mainly from the aspect of corrosion fatigue analysis [4,5], stress corrosion cracking [6], strain influence on corrosion [7], hydrogen embrittlement [8], and the stability of the passive layer developed under mechanical stress [9]. Anodic protection involving raising the potential of the protected metal to its passive zone for the formation of a passive thin layer on its surface has not been performed on HSHCsw embedded in concrete until present. Thus, it is of great interest to study the range of anodic potentials (APs) and the duration that could be adopted in the function of Cl⁻ concentrations to avoid uncontrolled application that would lead to structural breakdown.

It is known that a newly made concrete has a pH of about 12.5–13.2 due to the release of calcium hydroxide during hydration and the presence of sodium and potassium hydroxides in the pore solution [10]. The high pH range of concrete can prevent steel corrosion by promoting the formation of gamma ferric oxide (γ -Fe₂O₃) acting as passive film [11,12]. If the passivation is not disturbed, the protection of embedded steel will continue and the durability of concrete structure could last forever.

In reality, the concrete is porous [13,14] and susceptible to the ingress of Cl⁻ especially from the marine environment and de-icing salt in cold climates during its service [15]. In addition, Cl⁻ under a threshold level could have been introduced into concrete through the use of recycled aggregates [16] and the mixing of water

^{*} Corresponding author: Siaw Foon Lee, Spanish National Research Council, Eduardo Torroja Institute for Construction Science (IETcc-CSIC), Madrid, Spain, e-mail: siawfoon@ietcc.csic.es

^{*} Corresponding author: Seong Shan Yap, Faculty of Engineering, Multimedia University, Jalan Multimedia, 63100 Cyberjaya, Selangor, Malaysia, e-mail: seongshan@gmail.com

Jose Fullea García: Spanish National Research Council, Eduardo

Torroja Institute for Construction Science (IETcc-CSIC), Madrid,
Spain

during concrete manufacturing. Many studies have shown that the presence of Cl⁻ can lead to the initiation of pitting corrosion on the steel [17] at the pH range of concrete. For instance, the absorption of Cl- via intergranular boundaries of the passive layer will lead to the breakdown of the film [18]. In the case of TiN inclusion used to increase the drawability of steel, the steel matrix surrounding TiN will undergo anodic dissolution when it is exposed to NaCl electrolyte. Due to the fact that it is insoluble and electronic conductor, these properties allow TiN to act as cathodic site and will remain in the inner part of the pit. Thus, an occluded passive film is hardly formed to fully cover up TiN and a step-like pit will then be formed. Due to an extreme gradient of a high Cl⁻ concentration in the electrolyte, a large influx of aggressive Cl⁻ would appear between the inner pit and NaCl bulk electrolyte [19]. On top of that, the combination of Cl⁻ and the passive oxide could form Cl⁻ complexes leading to the volume expansion and the breakdown of the film [20].

However, Scott [21] reported that the passivation on bare steel rods can be maintained in Cl^- contaminated saturated $Ca(OH)_2$ or cement-saturated solutions provided that free oxygen gas is excluded from the steel surface. On the other hand, Hausmann [22] showed that there exists a critical Cl^- concentration that should not be surpassed in the oxygen free $Ca(OH)_2$ saturated electrolyte for the steel surface not showing any corrosion.

In view of the above facts, HSHCsw with 0.82% carbon, Young's modulus of 200 GPa and yield strength of 1,300 MPa, extensively used in the construction in Spain, was adopted in this work. First, the open circuit potential (OCP) measurement and the cyclic potentiodynamic polarization (CPP) were performed on HSHCsw to investigate its sustainability to which limit of the amount of Cl⁻ could be present in a high alkaline deaerated electrolyte without leading to pitting corrosion. With the obtained range of the allowable limit of Cl⁻ concentration, anodic potentiostatic application (APA) within the passive zone was applied on HSHCsw for 48 h. The purpose was to view how the presence of the Cl⁻ amount could influence the selection of the range of anodic potentials (APs) and the rate of corrosion during the passive period before pitting corrosion starting to take place in APA. The comparison between the gravimetrically-calculated and theoretically-calculated mass loss was made. The mechanism leading to pitting corrosion under APA in very high alkaline deaerated electrolyte was also proposed. This work could provide a thorough information in reducing the risk of accidentally implementing the AP outside the safety margin that could lead to the structural breakdown under anodic protection.

Table 1: Chemical composition of HSHCsw adopted in this study

С%	Mn%	Si%	Р%	S %	Cr%	Fe%
0.82	0.65	0.17	<0.015	0.022	0.28	98.04

2 Experimental method

2.1 Materials and electrolytes

As-received HSHCsw of plain surface with a diameter of 8 mm from the company of EMESA (Arteixo, La Coruña, Spain) was adopted in this study with its chemical composition presented in Table 1. The steel wire was cut into 10 cm long. Before the electrochemical measurements, the steel wires were ultrasonically cleaned in a cleaning solution for around two minutes to remove zinc phosphate (ZnPO₄) that was coated on its surface during fabrication. The cleaning solution is made from hydrochloric acid and water in a proportion of 1:1 together with a corrosion inhibitor called hexamethylenetetramine of 3 g/L. The steel wires were then rinsed in the running tap water and dried in air with a hair dryer. The clean steel wires were covered with adhesive tapes on both sides, as shown in Figure 1, with the exposed surface of 3 cm in length. As soon as the steel wires were dried with the hair dryer, an air-formed film of gamma ferric oxide (γ-Fe₂O₃) with a thickness of 10–20 Å was formed on the steel surface [23,24]. All steel wires were kept in a sealed bag to avoid the humidity in the air before they were used in the test the following day.

Electrolyte at pH 13.4 was made by dissolving saturated $Ca(OH)_2$ and 0.5 M KOH in distilled water. Different amounts of NaCl was added to the electrolyte in order to have the Cl^- concentration of 0.1 M, 0.25 M (brackish water), 0.5 M (sea water), 1 M (severe marine environment), and 2 M and 3 M (extremely severe marine environment).

2.2 Electrochemical measurements

Figure 2 shows the schematic drawing of the electrochemical cell used in this study. The cell had four holes on



Figure 1: Sample of HSHCsw with black-colour adhesive tapes on both sides.

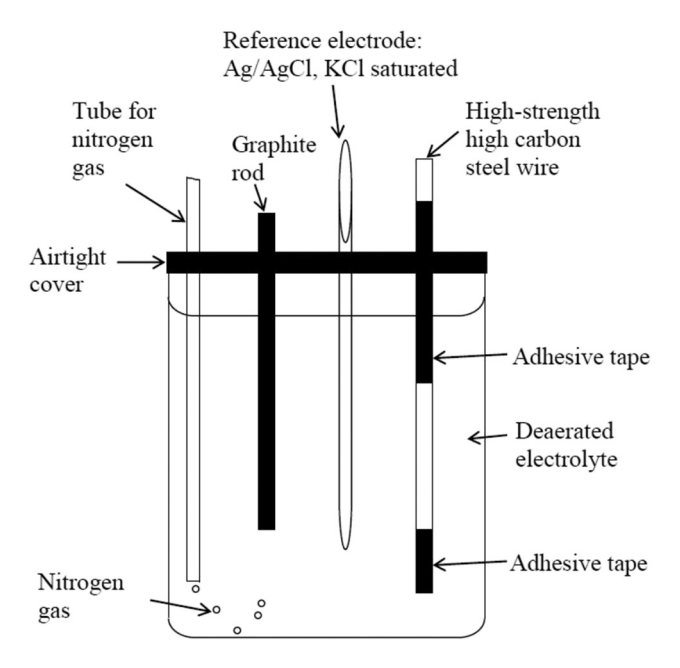


Figure 2: Schematic drawing of the electrochemical cell.

the top of the airtight cover to allow the introduction of the reference electrode, the counter electrode, the working electrode, and the tube of nitrogen gas into the electrolyte. In the electrochemical measurement, the working electrode was the HSHCsw, the counter electrode and the reference electrode were a graphite rod and Ag/AgCl in saturated KCl, respectively. Before the steel wire was introduced in the cell, nitrogen gas was bubbled through the electrolyte for 20 min to purge oxygen gas from the electrolyte until the oxygen concentration of electrolyte reached \leq 0.5 ppm, which was measured using the Clark electrode. A flowmeter was used to control the flow rate of nitrogen gas that was able to maintain the oxygen concentration of electrolyte at \leq 0.5 ppm throughout the electrochemical test.

The corrosion potential $(E_{\rm corr})$ of the steel wire was measured continuously for 3 days using OCP measurement and the equipment used was the Agilent 34970A data logger. The measurement of $E_{\rm corr}$ was started straight away after the steel was introduced into the deaerated electrolyte. As for CPP and APA, the ACM instruments with serial no. 1127 and the Gill AC with serial no. 1127 sequencer software were employed. For CPP measurement, the potential starting from -900 to +600 mV as a reverse potential at a scan rate of 10 mV/min was applied to the steel wire. Application of CPP allows the determination of whether HSHCsw would undergo domains of immunity, active $E_{\rm corr}$, passive and transpassive with pitting potential $(E_{\rm pit})$ caused by ${\rm Cl}^-$ in deaerated electrolyte at pH 13.4. Thus, additional tests of CPP in the extremely severe marine

environment of 2 and 3 M Cl⁻ deaerated electrolyte were also performed to examine their influence on the passivation of steel wire. The CPP curves were reversed at +600 mV for the purpose of the uniformity of potential scale in CPP-curve comparison under different Cl⁻ concentrations in the deaerated electrolyte. For APA, APs with an interval of 50 mV within the determined passive region were applied to the steel wire for 48 h. All tests were performed at the room temperature of 21°C. After APA test, the electrolytes were analysed to find out the quantity of Fe²⁺/Fe³⁺ escaped into the deaerated electrolytes during the test using the inductively coupled plasma (ICP) technique. The instruments used was Varian 725-ES Optical Emission Spectrometer ICPE, with the potential being set to be 1.40 kW, the plasma flow of 15 L/min, auxiliary flow of 1.50 L/min, and the mist flow of 0.80 L/min. The unit shown by ICP technique was in ppm and then converted into gram. The surface morphology was examined under the light microscope (Nikon SMZ-2T Japan) with eyepiece at $10 \times /16$. The microstructure of corrosion products was studied under the scanning electron microscope (SEM) (S-4800, Hitachi) and the energy dispersive X-ray spectroscopy (EDS) was performed on them.

3 Results and discussion

3.1 $E_{\rm corr}$

Figure 3 shows E_{corr} of HSHCsw at open circuit in 4 different Cl⁻ concentrations over a 3-day period in the deaerated electrolyte at pH 13.4. The four curves have the same characteristic trend, which is, the E_{corr} drift towards positive direction on immersion [25], then reverse and towards negative, eventually drift back towards more positive, and finally all reach a constant value of around -400 mV. Steel wire showing different shifts of $E_{\rm corr}$ in the time range of 2-65 h is mainly due to the different Cl⁻ concentrations, not due to the absence of free oxygen gas on the steel wire surface [22]. In this work, an airformed film y-Fe₂O₃ [24] was present on the surface before it was introduced into the electrolyte. On immersion, the air-formed film tends to breakdown at its weak points and Fe dissolves into Fe²⁺ through anodic reaction at these points. Due to the fact that free oxygen gas is completely purged from the electrolyte by the continuous flow of N₂, the cathodic reaction involving oxygen gas and water does not really takes place on the steel wire surface to produce OH⁻ as shown by the chemical reaction of $\frac{1}{2}O_2 + H_2O + 2e^- = 2OH^-$ [19]. Instead, the released

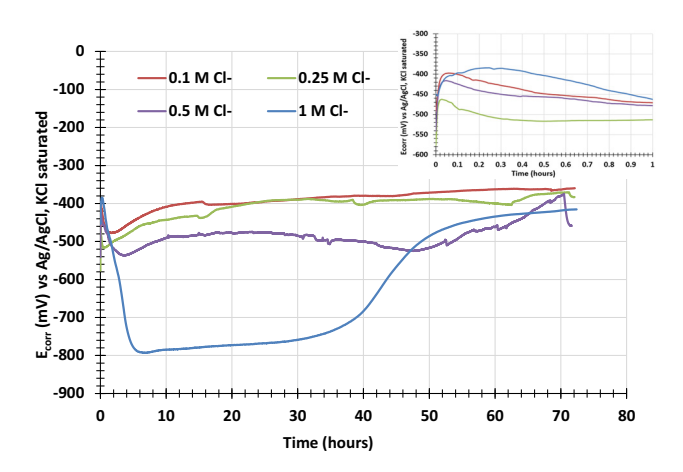


Figure 3: E_{corr} of HSHCsw at open circuit in deaerated electrolytes at pH 13.4 at 0.1, 0.25, 0.5, and 1 M Cl⁻ over a 3-day period. Right top is the magnifying graph of the first hour of immersion.

Fe²⁺ immediately combines with OH⁻ coming from the deaerated electrolyte to form passive film ferrous hydroxide (Fe(OH)₂) to reinforce the weak points found at the air-formed film. This explains why $E_{\rm corr}$ moves towards positive direction within the first minute of immersion, as seen in the built-in magnifying graph on the right top in Figure 3. However, the coexistence of Cl⁻ in the electrolyte can induce more weak points at the air-formed film, and thus, it causes $E_{\rm corr}$ drift towards negative direction. It can be seen that the higher the concentration of Cl⁻ is, the more negative the $E_{\rm corr}$ becomes.

At 1 M Cl $^-$, due to a considerably high Cl $^-$ concentration that leads to the generation of relatively high susceptible areas in the air-formed film, the $E_{\rm corr}$ takes longer time to reach -400 mV. The maximum negative value of $E_{\rm corr}$ reached was -793 mV vs Ag/AgCl, saturated KCl, which is equivalent to -594 mV vs standard hydrogen electrode (SHE). From the Pourbaix diagram of steel [26] in Figure 4, -594 mV vs SHE still falls within the passivation zone of steel, not in the small zone of corrosion that appeared at very high alkaline pH. Somehow, due to the high alkaline and deaerated conditions, the formation of passive film becomes faster than the attack of Cl $^-$ with time. Thus, all the $E_{\rm corr}$ move back towards positive direction and settle at around -400 mV.

During the test, the steel wire surfaces were inspected visually for any possible appearance of rust. It was found that at the end of the test the steel wires remained bright. In order to ensure that no tiny dots of rust appeared on the surface that failed to be spotted visually, the steel wires were examined under the light microscope after the tests, again no visible corrosion was noticed on the steel wire surface with the Cl⁻ concentration as high as 1 M in the deaerated electrolyte at pH 13.4. The absence of oxygen

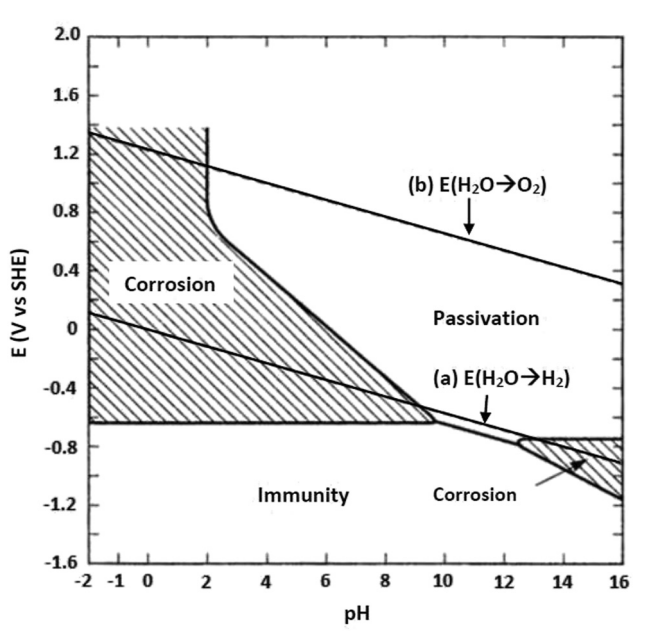


Figure 4: Pourbaix diagram for steel showing the zone of immunity, corrosion, and passivation. Equation for (a): $E(\text{water} \rightarrow \text{H}_2) = 0.000 - 0.0591$ pH. Equation for (b) $E(\text{water} \rightarrow \text{O}_2) = 1.228 - 0.0591$ pH [26].

gas and the presence of high concentration of OH^- kept the produced $Fe(OH)_2$ as it was without being oxidised further to ferric compound that having a cubic structure indistinguishable from the air-formed film at room temperature [11,27].

3.2 CPP

Figure 5 shows the CPP curves of steel wires at four different Cl⁻ concentrations in deaerated electrolyte at pH 13.4. No cathodic cleaning at -1,200 mV was performed in order to maintain the air-formed film of y-Fe₂O₃ on the surfaces of all steel wires before the scanning started. It can be seen that for Cl⁻ concentrations below 0.5 M, the corresponding current densities of reverse curves (dotted lines) are lower than those of forward curves (solid lines), the reverse curve (dotted line) superimposed on the forward curve (solid line) only at 1 M Cl-. All the curves reveal negative hysteresis loops with the repassivation potential (E_{rep}) above the active E_{corr} on the CPP curves [28]. In addition, no sudden increase in current densities related with E_{pit} is seen on the CPP curves. All these curve characteristics reveal that no pitting corrosions took place on the steel wire surface during the CPP scanning [29]. There was no sharp increase in the current for Cl⁻ concentration below 1 M even at +237 mV (vs Ag/AgCl, sat KCl), at

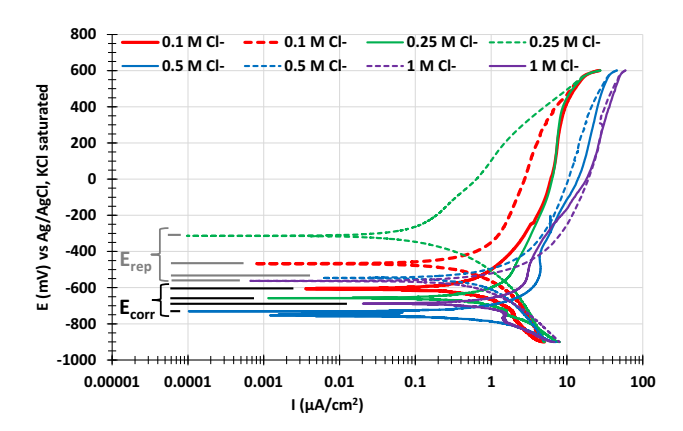


Figure 5: CPP of HSHCsw in deaerated electrolytes at pH 13.4 at 0.1, 0.25, 0.5, and 1 M Cl⁻. A complete CPP from –900 to +600 and then back to –900 mV was performed for each Cl⁻ concentration. Forward curves are plotted as solid lines and reverse curves are plotted as dotted lines for easy viewing and comparing.

which the oxygen gas is theoretically produced from water. It is because that the high pH 13.4 together with the continuous flowing of nitrogen gas to purge the generated oxygen gas do not encourage active pitting corrosion on the steel surface. All steel wires remained bright throughout the test and no visible corrosion was noticed under the light microscope after the test. Since the potential is scanned from cathodic condition, the active $E_{\rm corr}$ on the CPP curves become more negative than the constant $E_{\rm corr}$ achieved at open circuit as shown in Figure 3, which are in agreement with previous study [30].

According to Figure 3, the achieved constant $E_{\rm corr}$ at open circuit is -400 mV. Thus, the passive current densities at -400 mV on CPP in Figure 5 are noted and they are 1, 1.8, 4, and 4.8×10^{-6} A/cm² for 0.1, 0.25, 0.5, and 1 M Cl⁻, respectively. These values are in fact lower when compared to the passive current density of 3×10^{-5} A/cm² reported by Shi *et al.* [30] for low alloyed and low carbon reinforcing steels at 0.1 M Cl⁻ in aerated simulated concrete pore solution.

In addition, CPP scan was also performed on the steel wire at 2 and 3 M Cl $^-$ with $E_{\rm pit}$ shown at +395 and +67 mV vs Ag/AgCl, respectively, as seen in Figure 6, which are equivalent to +600 and +272 mV vs SHE, respectively. According to the Pourbaix diagram for steel in Figure 4, it is obvious that $E_{\rm pit}$ at 2 M Cl $^-$ falls in the oxygen evolution region and that of 3 M Cl $^-$ falls in the passivation region. It can be seen that the generation of oxygen gas from the oxygen evolution reaction ($E_{\rm oe}$) (40H $^ \rightarrow$ O $_2$ + 2H $_2$ O + 4e $^-$) [29,31] at + 395 mV vs Ag/AgCl is higher than the purging of oxygen gas by nitrogen gas. Thus, the presence of oxygen gas together with Cl $^-$ in the electrolyte encourage pitting corrosion to take place on the steel wire surface at 2 M Cl $^-$. This fact is supported by the report of

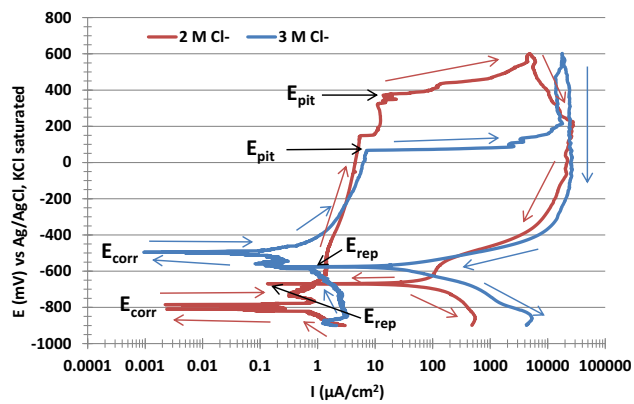


Figure 6: CPP of HSHCsw in deaerated electrolytes at pH 13.4 at 2 and 3 M Cl⁻.

Scott [21] that the presence of oxygen gas in the electrolyte at pH 12 together with a high $\rm Cl^-$ concentration could force a steel to corrode. However, at 3 M $\rm Cl^-$, $E_{\rm pit}$ occurs even without the presence of free oxygen gas this could be due to that a critical $\rm Cl^-$ concentration has been surpassed in the deaerated electrolyte [22] or the formation of soluble complex ions between $\rm Cl^-$ and cations leading to the breakdown of passive film [32].

Both CPP curves at 2 and 3 M Cl $^-$ present a big positive hysteresis loop, indicating the occurrence of lots of pitting corrosions on the steel wire surface [33]. Such big positive hysteresis loop makes the reserve anodic current struggle to decrease or to stop pit propagation at the beginning of the reverse scan. Finally, at 2 M Cl $^-$, the reserve anodic current changes to reverse cathodic current at $E_{\rm rep}$ falling in the transition region of the corresponding forward curve at $-670\,\mathrm{mV}$ [34, 35], while at 3 M Cl $^-$, $E_{\rm rep}$ fall in the cathodic region of the corresponding forward curve at $-574\,\mathrm{mV}$ [36]. The big hysteresis loop together with $E_{\rm rep}$ not falling in the passive region indicate the difficulty in repassivating all the active pits to restore a complete passive layer [33], and also, there possibly exists a high tendency of HSHCsw under further attack of pitting corrosion.

It is obvious that HSHCsw is susceptible to pitting corrosions at both 2 and 3 M Cl⁻ deaerated electrolytes at pH 13.4. However, it is more corrosion resistant at 2 M Cl⁻ because $E_{\rm pit}$ at 2 M Cl⁻ is higher than $E_{\rm pit}$ at 3 M Cl⁻ [36] and the plateau of passive region at 2 M is also wider than 3 M Cl⁻ [37].

3.3 APA

The purpose of APA within the passive zone is to regenerate passive film on the steel surface in order to decrease the rate of corrosion. However, the application of APA

without proper control would lead to severe corrosion. Since $E_{\rm pit}$ for Cl $^-$ concentration below 1 M is not shown in the CPP in Figure 5, the potential that would lead to the theoretical decomposition of water to oxygen gas based on the equation shown in Figure 4 is calculated and thus used as the upper limit in order to preserve the deaerated condition in the electrolyte. It is found to be $E_{\rm (water \to O_2)} = +436$ mV (vs SHE) or +237 mV (vs Ag/AgCl, sat KCl) at pH 13.4. The lower limit of passive region is taken as -400 mV, which is the $E_{\rm corr}$ constant achieved at open circuit in Section 3.1. Therefore, the passive region between -400 and +100 mV was determined for the study of APA.

Table 2 shows the gravimetric (Exp) and the theoretical mass loss (Theo) of HSHCsw after the 48 h APA in deaerated electrolyte at pH 13.4 at 0.1, 0.25, 0.5, and 1 M $\rm Cl^-$, calculated based on the equations (1) and (2) in Section 3.3.1. The bold digits referring to that pitting corrosion was observed on the steel wire after the 48 h APA test. The ICP technique showed that the maximum quantity of $\rm Fe^{2+}/\rm Fe^{3+}$ detected in the electrolyte was 3.5 \times 10⁻⁶ g for the cases that had pitting corrosions after 48 h. This value is negligible and this indicates that all the released $\rm Fe^{2+}/\rm Fe^{3+}$ involve in the precipitation as solid oxides on the HSHCsw surface. Most of the steel wires that did not show pitting corrosion had quantity of $\rm Fe^{2+}/\rm Fe^{3+}$ below the detected value (<LD).

3.3.1 Relationship between AP, passive period, rate of corrosion, mass loss, and Cl⁻ concentration

The 48 h AP that induced pitting corrosion on HSHCsw as shown in Table 2 (bold digits) is plotted *versus* the

corresponding Cl⁻ concentration in Figure 7, with -400 mV marked as E_{corr} . The curve can be represented by a seconddegree polynomial equation as $y = 469.61x^2 - 1029.7x +$ 208.48 with R^2 being 0.995. This equation can only be used as an interpolation for a range of Cl⁻ concentration between 0.1 and 1 M in deaerated electrolyte at pH 13.4 in this study. It shows that HSHCsw will not corrode in the presence of Cl⁻ when the AP below the curve is applied within the time frame of 48 h. However, if the AP above the curve is applied, pitting corrosion will develop on HSHCsw. At 1 M Cl⁻, the AP that does not lead to pitting corrosion has a narrow margin, around 50 mV from $E_{\rm corr}$. Thus, APA within passive zone to reproduce passive film to reduce the rate of corrosion on the steel wire surface will not work well when the presence of Cl⁻ concentration is very high or in the old concrete that has narrow passive zone due to pH lower than 11.5 [38].

The curves of anodic current density (I_a) against time for HSHCsw showing no pitting corrosion at 0.1 M and 0.25 M Cl⁻ at -200 mV (electrochemical conditions below the curve in Figure 7) are displayed in Figure 8. It is found that I_a oscillates between 0.3 and 1 μ A/cm² and between 1 and 2.5 μ A/cm² at 0.1 and 0.25 M Cl⁻, respectively, higher than that reported by other reinforcing steel in the aerated electrolyte [25]. Although this is the case, no pittings are generated on HSHCsw. It is mainly because AP is applied within the passive region, in addition to the high alkaline deaerated electrolyte. Furthermore, continuous repassivation is found occurring on HSHCsw during APA because lots of current transients are clearly seen on the curves.

Figure 9(1(a), 2(a), 3(a), and 4(a)) shows the $I_a vs$ time for 0.1, 0.25, 0.5, and 1 M Cl⁻, respectively, corresponding

Table 2: Gravimetric (Exp) and theoretical mass loss (Theo) of HSHCsw and the released Fe²⁺/Fe³⁺ in the deaerated electrolytes at pH 13.4 after 48 h APA measurement

		Anodic potential (mV)								
Cl ⁻ (M)		-400	-350	-300	-250	-200	-100	0	+100	
0.10	Exp (g)	0.0018		0.0052		0.0027	0.0064	0.0071	0.1111	
	Theo (g)	0.0004		0.0006		0.0002	0.0004	0.0007	0.0861	
	Fe^{2+}/Fe^{3+} (×10 ⁻⁶ g)	<ld< td=""><td></td><td><ld< td=""><td></td><td>0.0031</td><td><ld< td=""><td><ld< td=""><td>0.0870</td></ld<></td></ld<></td></ld<></td></ld<>		<ld< td=""><td></td><td>0.0031</td><td><ld< td=""><td><ld< td=""><td>0.0870</td></ld<></td></ld<></td></ld<>		0.0031	<ld< td=""><td><ld< td=""><td>0.0870</td></ld<></td></ld<>	<ld< td=""><td>0.0870</td></ld<>	0.0870	
0.25	Exp (g)	0.0040		0.0046		0.0024	0.0058	1.4854		
	Theo (g)	0.0004		0.0004		0.0006	0.0006	1.5897		
	Fe^{2+}/Fe^{3+} (×10 ⁻⁶ g)	<ld< td=""><td></td><td><ld< td=""><td></td><td><ld< td=""><td><ld< td=""><td>1.0430</td><td></td></ld<></td></ld<></td></ld<></td></ld<>		<ld< td=""><td></td><td><ld< td=""><td><ld< td=""><td>1.0430</td><td></td></ld<></td></ld<></td></ld<>		<ld< td=""><td><ld< td=""><td>1.0430</td><td></td></ld<></td></ld<>	<ld< td=""><td>1.0430</td><td></td></ld<>	1.0430		
0.50	Exp (g)	0.0032		0.0048	0.0081	0.8164		2.7193		
	Theo (g)	0.0006		0.0011	0.0008	0.8846		2.7248		
	Fe^{2+}/Fe^{3+} (×10 ⁻⁶ g)	<ld< td=""><td></td><td>0.0025</td><td><ld< td=""><td>0.5636</td><td></td><td>1.5530</td><td></td></ld<></td></ld<>		0.0025	<ld< td=""><td>0.5636</td><td></td><td>1.5530</td><td></td></ld<>	0.5636		1.5530		
1.00	Exp (g)	0.0030	0.1553	0.1796		2.8013		4.1319		
	Theo (g)	0.0017	0.1567	0.1836		2.9354		5.0391		
	Fe^{2+}/Fe^{3+} (×10 ⁻⁶ g)	0.0179	0.1633	0.0397		1.6115		3.5000		

Bold digits refer to steel wire having pitting corrosions and <LD refer to below the detected value.

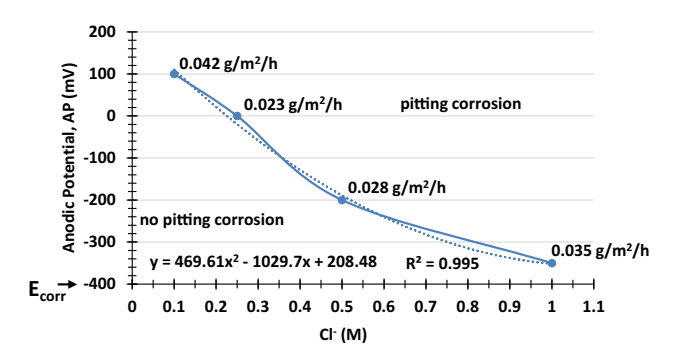


Figure 7: Relationship between AP inducing pitting corrosion on HSHCsw within 48 h time frame and Cl^- concentration in deaerated electrolyte at pH 13.4 with the interpolation equation being applied only to the range of Cl^- concentration from 0.1 to 1 M, with -400 mV marked as E_{corr} as in Figure 3. The rate of corrosion corresponding to each point on the curve is calculated based on equation (3) in this article.

to the points plotted on the curve of AP *versus* Cl⁻ in Figure 7 that provides the second-degree polynomial equation as $y = 469.61x^2 - 1029.7x + 208.48$ with R^2 being 0.995. The passive period in the graph is referred to the duration before the generation of active pitting corrosion. It can be seen that pitting corrosion does not appear immediately upon the application of AP; instead, it took some time to appear. A sudden drop in the I_a after 30 h at 0.25 M Cl⁻ in Figure 9(2(a)) was because of a thick layer of solid oxides formed on the whole steel wire surface starting to act as a protective layer in preventing further active pitting corrosion.

The passive period *versus* AP for 0.5 and 1 M Cl⁻ was then plotted in Figure 10. A non-linear relationship between the passive period and AP is obtained. Somehow, it is clear that the passive period decreases when AP becomes more positive, and increases when the Cl⁻ concentration becomes less.

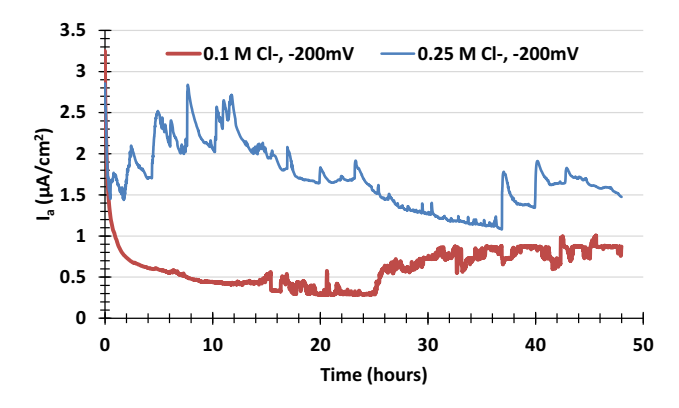


Figure 8: Anodic current density (I_a) of HSHCsw at 0.1 and 0.25 M Cl $^-$ when the AP is polarized at -200 mV (in the zone of no pitting corrosion in Figure 7), in the deaerated electrolyte at pH 13.4.

Since steel wire is usually embedded in the concrete structure and the APA involves the dissolution of iron to form passive film, it is interesting to find out theoretically the amount of iron that has been consumed during the APA application. Thus, the gravimetric mass loss of corroded HSHCsw from the APA and the theoretical mass loss calculated using Faraday's law is compared. The gravimetric mass loss, $m_{\rm e}$, was obtained by subtracting the mass of HSHCsw after the test, $m_{\rm l}$, from that before the test, $m_{\rm l}$, in grams.

$$m_{\rm e}=m_0-m_1. \tag{1}$$

The theoretical mass loss in grams, m_F , was calculated using Faraday's law as below:

$$m_{\rm F} = \frac{MIt}{zF},\tag{2}$$

where *M* is the molecular weight of metal (M = 56 g/molfor Fe), z is the valence number of ion (z = 2 for Fe), F is the Faraday constant ($F = 96.485 \, \text{C/mol}$), I is the density of current in A/cm^2 , and t is the corrosion duration in seconds. "It" was calculated by integrating the curve of I_a against time obtained from the APA as exemplified in Figure 9(1(a), 2(a), 3(a), and 4(a)). The relationship between the gravimetrically and the theoretically calculated mass loss of HSHCsw versus the Cl⁻ concentration at different APs is shown in Figure 11. From the comparison, it can be seen that Faraday's law is only valid to predict the mass loss of HSHCsw when no severe pitting corrosion occurs. The prediction starts to deviate when severe corrosion occurs, especially at 1 M Cl⁻ at +0 mV where the theoretically-calculated mass loss of HSHCsw is 21.96% higher than the gravimetrically-calculated value.

Due to the fact that the prediction of mass loss from Faraday's law is only valid when there is no severe pitting corrosions, the rate of corrosion ($R_{\rm corr}$) in g/m²/h of each point on the curve in Figure 7 was then calculated within the passive period using the following equation:

$$R_{\rm corr} = \frac{m_{\rm F}}{A \cdot t},\tag{3}$$

where A is the specimens area in square meters, t is the passive period as defined in Figure 9(1(a), 2(a), 3(a) and 4(a)), and $m_{\rm F}$ is the mass loss within the passive period that was calculated using Faraday's law in equation (2). The calculated rates of corrosion before the occurrence of active pitting corrosion is found between 0.023 and 0.042 g/m²/h, no track of the influence of the different Cl⁻ concentration on it. These rates of corrosion of HSHCsw in deaerated electrolyte at pH 13.4 when no pitting corrosion occurs under APA are a lot lower than the rate of corrosion of stainless steel under the stand-alone polyaniline (PANI) protection in 5 M H₂SO₄, which is 0.833 g/m²/h [39].

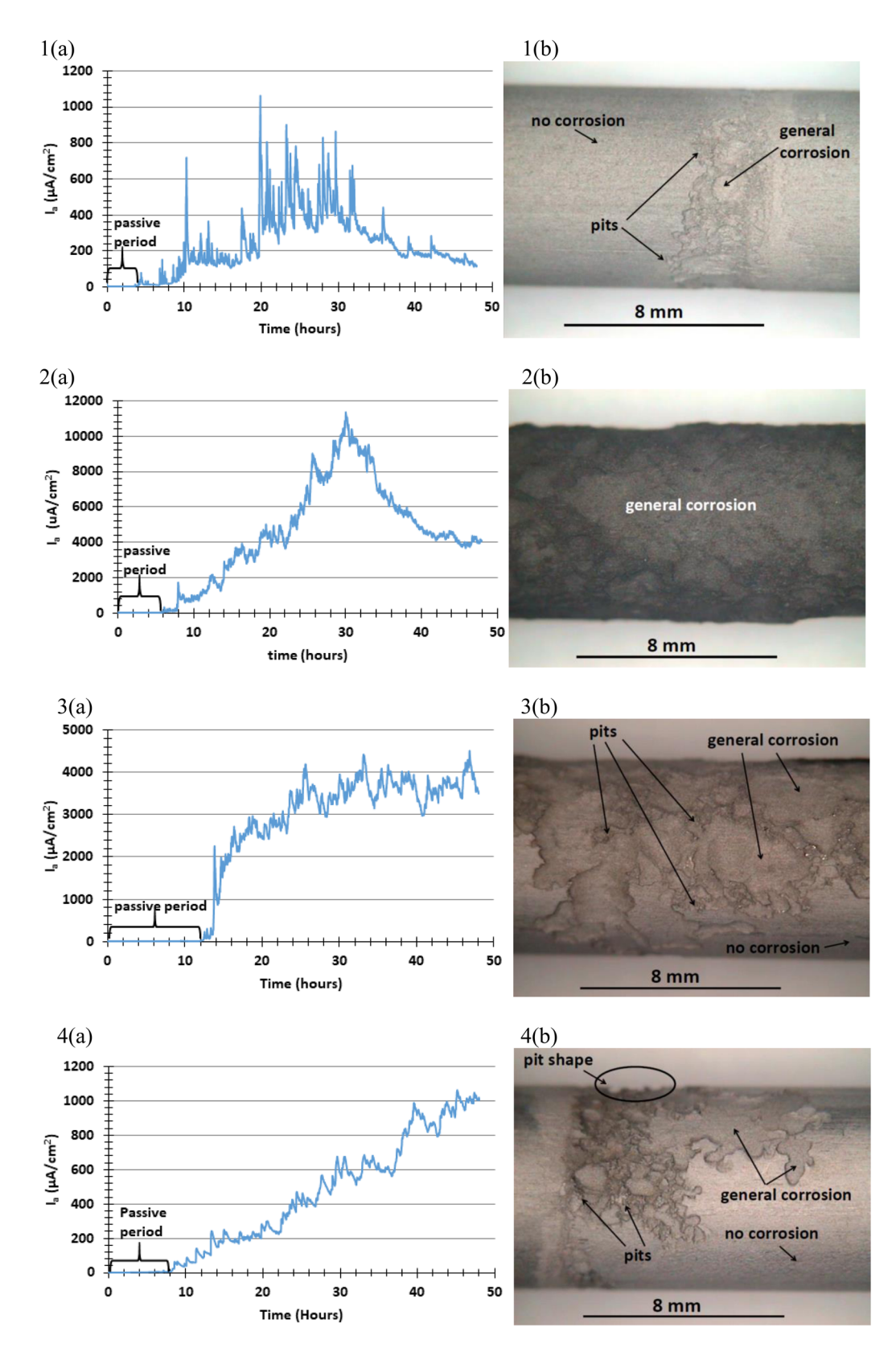


Figure 9: I_a of HSHCsw during 48 h in deaerated electrolyte at pH 13.4 and its corresponding surface morphology (light microscope: 15×) at: (1a and 1b) 0.1 M Cl⁻ and +100 mV, (2a and 2b) 0.25 M Cl⁻ and +0 mV, (3a and 3b) 0.5 M Cl⁻ and -200 mV, and (4a and 4b) 1 M Cl⁻ and -350 mV, corresponding to the points plotted on the curve in Figure 7.

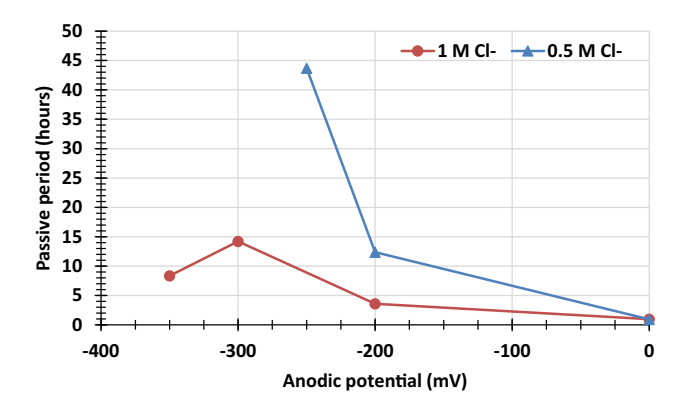


Figure 10: Relationship of passive period vs AP for HSHCsw in deaerated electrolyte at pH 13.4 at 0.5 and 1 M Cl $^-$.

The pit morphologies corresponding to the points plotted on the curve of AP versus Cl in Figure 7 on HSHCsw at different Cl⁻ concentrations after APA, viewed under the light microscope (15x), are displayed in Figure 9(1(b), 2(b), 3(b), and 4(b)). It is different from small individual pits shown on the steel immersed in alkaline electrolyte at pH 12.5 under OCP [40]. Here many tiny or small pits are found amidst big and connected pits with no profound depth. The influence of Cl⁻ concentration together with AP on the number and the size of pits is evident. It can be seen that under both electrochemical conditions, which are the same AP but with the increase in Cl⁻ concentration or the same Cl⁻ concentration but with the increase in AP, will widen the pit size and cause the pits to be connected to each other and finally to become general corrosion.

The pit shapes of HSHCsw shown in Figure 9(4(b)) are similar to the reported pit shape of stainless steel and carbon steel [41]. Due to the fact that the pits were obtained after 48 h AP application, the pit depths are around between 0.18 mm (180 μ m) and 0.29 mm (290 μ m), which are deeper than the pit depth of stainless steels obtained from CPP [29,31], or carbon steel under 150 mV potentiostatics at pH 3.8 for 24 h [41]. For the case that undergoes severe corrosion leading to a complete general corrosion after 48 h AP application as shown in Figure 9(2(b)), the diameter of HSHCsw becomes around 0.44 mm (440 μ m) less than the original one, which is 8 mm.

Figure 12(a) shows the light micrograph $(60\times)$ of the as-received surface morphology of steel wire and Figure 12(b)–(d) shows the pits that appear on the steel wire surface at 1 M Cl⁻ and –200 mV, at 1 M Cl⁻ and –350 mV as well as at 0.5 M Cl⁻ and –200 mV, respectively. Comparing with the as-received surface morphology, Figure 12(b) reveals a lot of tiny pits due to the attack of Cl⁻ on the passive film [42]. The tiny pits

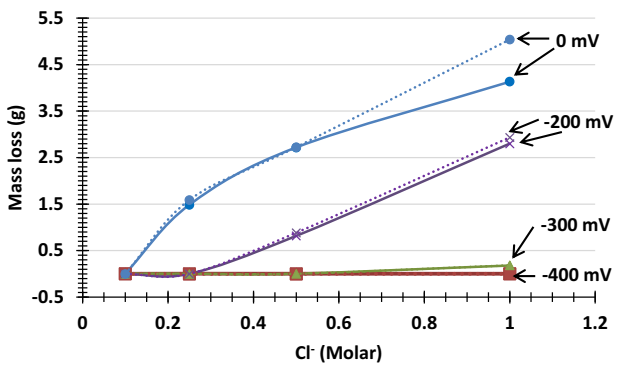


Figure 11: Gravimetrically-calculated (solid line) and theoretically-calculated (dotted line) mass loss of HSHCsw vs Cl⁻ concentration at different APAs within passive zone that lasted for 48 h.

within a big pit is also observed in Figure 12(c), which is not considered as the reported step-like pit in TiN inclusion [19] as Fe²⁺ and Fe³⁺ are soluble when iron undergoes oxidation. Thus, an occluded cover will be definitely formed to cover completely the big pit that contains tiny pits inside. Under active pitting corrosion, the tiny pits will merge to form even bigger pits, as shown in Figure 12(d). From the graphs of I_a vs time and light micrographs in Figure 9 as well as Figure 12, respectively, it can be deduced that when active pitting corrosions accidentally take place in APA, the individual tiny pit will not propagate deep into the steel wire to cause embrittlement [43,44]. Instead, they will tend to merge to form bigger pits leading to pseudo-general corrosions shown in Figure 9(2(b)). The expansion of corrosion products will also lead to the initiation of creviceinducing pits, encouraging more pseudo-general corrosions to take place on the steel wire surface [45].

3.3.2 Corrosion products and pit corrosion mechanism

Figure 13a shows the corrosion product produced on HSHCsw in the deaerated electrolyte (\leq 0.5 ppm) at pH 13.4 at 1 M Cl⁻ and -350 mV under the continuous flow of nitrogen gas. Semino and Galvele [46] reported that lepidocrocite (γ -Fe₂O₃·H₂O) oxide films (yellow brown) was the corrosion product formed on the pure iron in deaerated neutral NaCl electrolytes when AP below the $E_{\rm pit}$ was applied. However, from the colours of the corrosion product in this work, it is deduced that green rusts consisting of ferrous hydroxide Fe(OH)₂ (white) and ferric hydroxide Fe(OH)₃ (greenish) [47] actually appear on HSHCsw in the deaerated pH 13.4 electrolytes with the presence of NaCl.

Small bubbles are seen among the green rusts or on the steel wire surface close to the green rusts under active

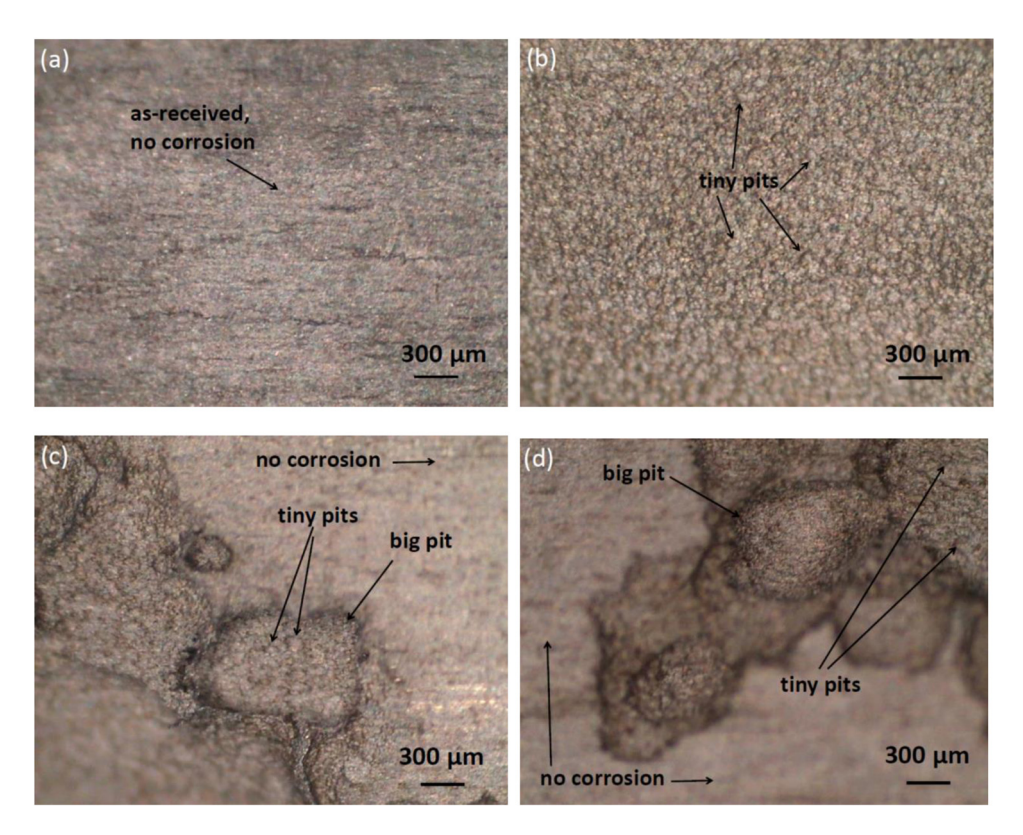


Figure 12: The light micrograph $(60\times)$ of the surface morphology of steel wire – (a) as-received, (b) pits at 1 M Cl⁻ and –200 mV, (c) pits at 1 M Cl⁻ and –350 mV, and (d) pits at 0.5 M Cl⁻ and –200 mV.

AP corrosion, as shown in Figure 13b, which was taken using borescope. The produced bubbles cannot be oxygen gas coming from the dissociation of water as the applied AP was well below the line b in the Pourbaix diagram in Figure 4. It is hydrogen gas as proposed by previous study [48].

When the electrochemical test was finished, the steel wire with green rust was removed from the deaerated electrolyte and left to expose to air at the room temperature of 21°C. The green rust was observed changing to dark brownish corrosion products, as shown in Figure 13(c). SEM image in Figure 13(d) and (e) shows that the corrosion products are a mix of magnetite Fe₃O₄ [49–51] and maghemite γ -Fe₂O₃ [52]. The EDS spectra in Figure 13(f) for magnetite Fe₃O₄ and Figure 13(g) for maghemite γ -Fe₂O₃ reveal the presence of the element Cl in the corrosion products supporting the fact that Cl $^-$ induced depassivation and also penetrated the passive film [53]. Very little of Na $^+$ and K $^+$ were present in the corrosion products due to the repulsive effect from the Fe $^{2+}$ and Fe $^{3+}$ inside the pits [53].

From the study of the corrosion products, the production of bubbles, and pit morphology, a schematic diagram of the pitting corrosion propagation as shown in Figure 14 together with the corresponding pitting

corrosion mechanism under APA are proposed. At the beginning, the application of AP causes Fe to dissolve into Fe^{2+} at the weak areas of air-formed passive film, as shown in Figure 14(a). The released Fe^{2+} will combine immediately with OH^- coming from the electrolyte to form the passive film of $Fe(OH)_2$, in Figure 14(b), to cover the weak point.

With further APA leading to active pitting corrosion, Fe from the bottom and the wall of the pit will dissolve not only into Fe^{2+} but also into Fe^{3+} . The dissolution of Fe from the pit wall will thus widen the pit size until individual pits connect to each other [40]. Due to the fact that the passive film is porous and the gradient concentration of Cl^- and OH^- existing between the bulk electrolyte and the trapped electrolyte, anions will penetrate the passive film and diffuse inside the pits [40], as shown in Figure 14(c). The generated Fe^{2+} and Fe^{3+} within the pits will react with OH^- in the trapped electrolyte as the chemical reaction below to form the green rust.

$$Fe^{2+} + 2OH^{-} = Fe(OH)_{2},$$
 (4)

$$Fe^{3+} + 3OH^{-} = Fe(OH)_{3}.$$
 (5)

In the alkaline medium, H₂O inside the trapped electrolyte or in the bulk electrolyte will go through the

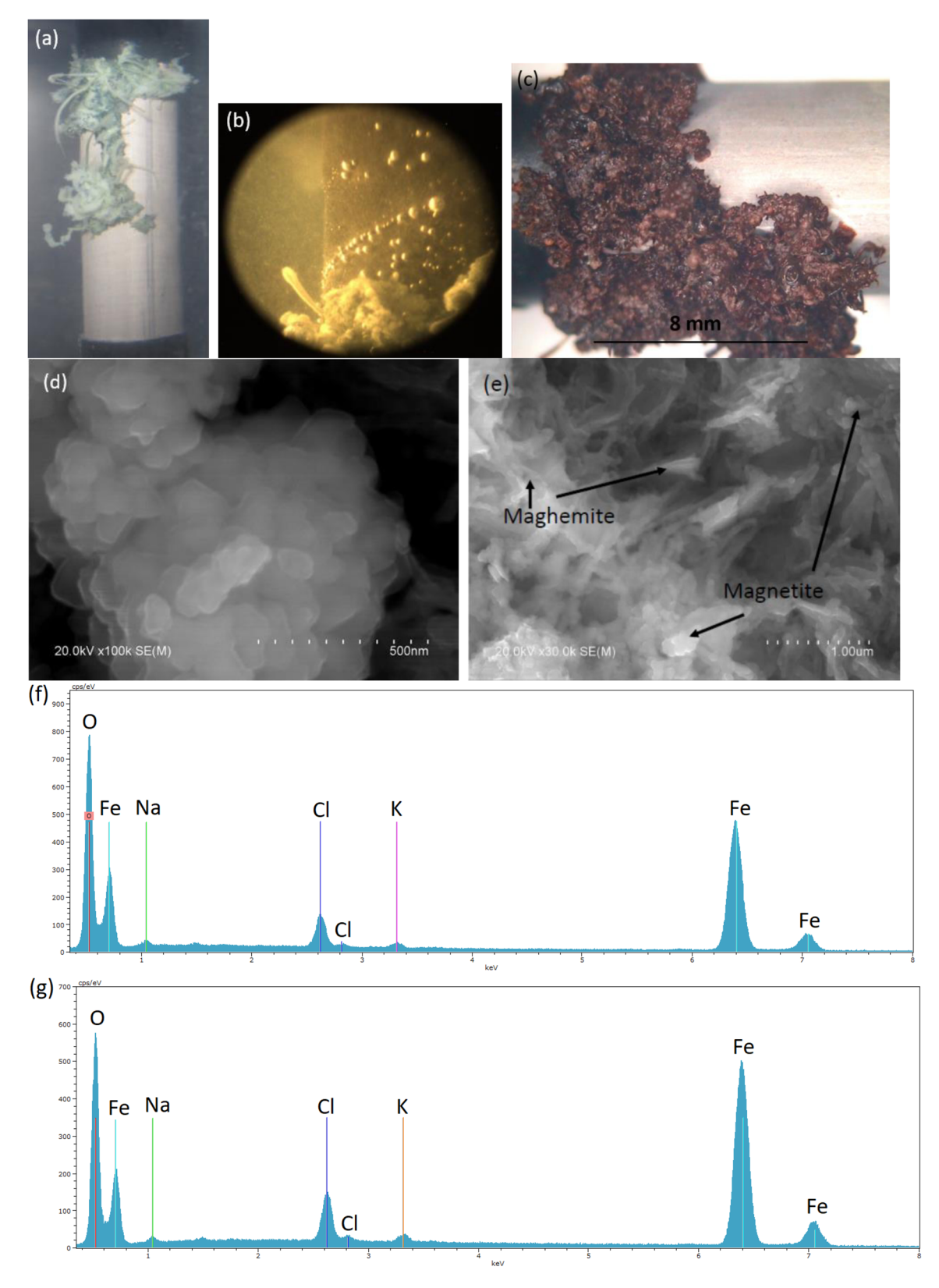


Figure 13: (a) Green rust – corrosion products of HSHCsw in deaerated (\leq 0.5 ppm in oxygen gas content) pH 13.4 electrolyte at 1 M Cl $^-$ and -350 mV taken by digital camera. (b) Hydrogen gas produced during active pitting corrosion taken by boroscope. (c) Brownish corrosion products (light microscope: $15\times$) – obtained after the green rust was exposed to air for some time. (d) SEM images of magnetite Fe₃O₄. (e) SEM images of magnetite Fe_3O_4 and magnemite γ - Fe_2O_3 . (f) The EDS spectrum of magnetite Fe_3O_4 . (g) The EDS spectrum of magnemite γ - Fe_2O_3 .

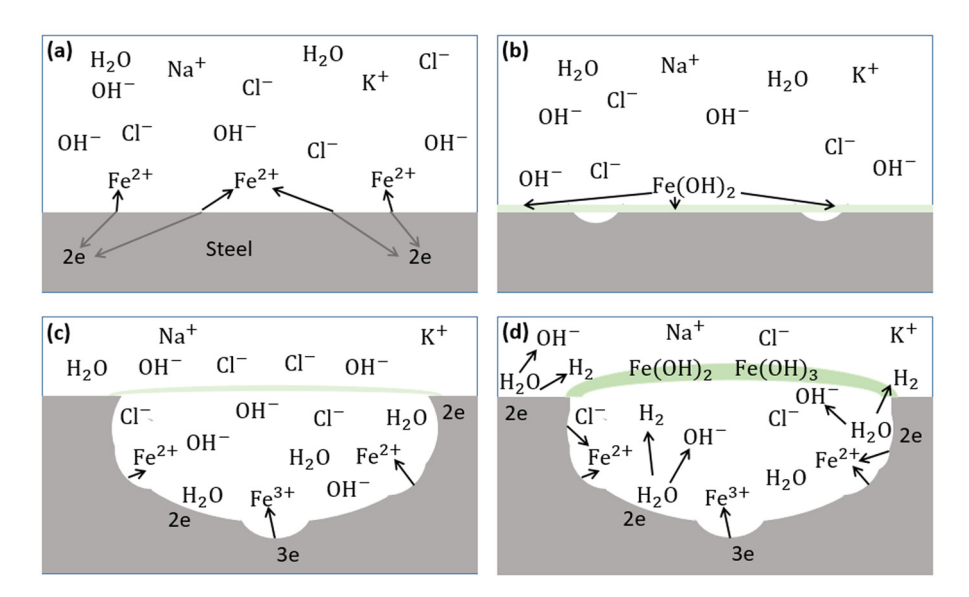


Figure 14: Schematic diagram of pitting corrosion mechanism under anodic potentiostatic application (APA). (a) Fe dissolving to Fe^{2+} at weak area of air-formed passive film. (b) Fe^{2+} combined with OH^- forming $Fe(OH)_2$ passive film. (c) Further dissolution of Fe to Fe^{2+} and Fe^{3+} and penetration of CI^- and OH^- from bulk to trapped electrolyte. (d) Formation of green rust $(Fe(OH)_2 + Fe(OH)_3)$ and H_2 .

following reaction with electrons that reach the steel wire surface to produce H_2 [48] as shown in Figure 14(d).

$$2H_2O + 2e = 2H_2 + 2OH^-.$$
 (6)

The generation of H_2 inside the trapped electrolyte together with Cl^- can cause local acidification. For iron, it proved theoretically and experimentally that a pH value of 3–4 can exist inside the trapped electrolyte of active pits [54]. When the green rusts become thick and impermeable leading to a complete consumption of the trapped electrolyte, I_a will drop as shown in Figure 9(2(a)) and the active corrosions will then terminate for the moment.

4 Conclusion

HSHCsw immersed in the high alkaline of pH 13.4 deaerated electrolyte (\leq 0.5 ppm) with different Cl $^-$ concentrations of 0.1, 0.25, 0.5, 1, 2 and 3 M was investigated for the possibility of pitting corrosion induced on the steel wire surface using the OCP, CPP, and APA. This study has shown that

- 1) HSHCsw can sustain in the presence of Cl⁻ as high as 1 M without pitting corrosion under the condition of OCP.
- 2) An inverse relationship between APs and Cl⁻ concentrations is found and can be represented with an interpolated second-degree polynomial equation as

- $y = 469.61x^2 1029.7x + 208.48$ with R^2 being 0.995, only for a range of Cl⁻ concentration between 0.1 and 1 M. This indicates that that HSHCsw will not corrode in the presence of Cl⁻ when AP below the curve is applied within the 48 h time frame. However, the application of AP above the curve will lead to the development of pitting corrosion on HSHCsw.
- 3) The theoretical prediction of mass loss after 48 h APA using Faraday's law will not be valid in the case of severe corrosion.
- 4) The corrosion products generated in the deaerated electrolyte at pH 13.4 during the APA are mainly Fe $(OH)_3$ (greenish) and $Fe(OH)_2$ (white) with hydrogen gas produced in adjacent areas or within active pits. The corrosion products will be turned into magnetite Fe_3O_4 and maghemite γ - Fe_2O_3 when they are exposed to air.
- 5) If the AP is accidentally applied outside the safety margin during the service of anodic protection, the initially generated corrosion will be pitting corrosion. However, further application of AP will not cause the pits to develop deep into the steel leading to embrittlement. The covering of corrosion products on the steel surface encouraging crevice corrosion together with the continuous AP application will induce the merging of pits and the dissolution of Fe from the pit wall. Thus, these phenomena will finally cause the initially generated pitting corrosions to appear as general corrosions on the steel surface.

Acknowledgements: David Hui appreciates the past and ongoing supports from NACE (New Orleans Section). The useful discussions with Charles Speed are acknowledged.

Funding information: Authors would like to thank the JAEDOC programme from the Spanish Research Council -El Consejo Superior de Investigaciones Científicas (CSIC).

Author contributions: All authors have accepted responsibility for the entire content of this manuscript and approved its submission.

Conflict of interest: David Hui, who is the co-author of this article, is a current Editorial Board member of Nanotechnology Reviews. This fact did not affect the peer-review process. The authors declare no other conflict of interest.

References

- Kamde DK, Manickam K, Pillai RG, Sergi G. Long-term performance of galvanic anodes for the protection of steel reinforced concrete structures. J Build Eng. 2021;42(103049):1-14.
- Prasad NKR, Pathak AS, Kundu S, Panchal P, Mondal K. The novel approach of sacrificial cathodic protection of mild steel in simulated concrete pore solution and concrete mortar by high phosphorus pig iron anodes. J Mater Res Technol. 2021:14:582-608.
- [3] Silva RS, Aleman C, Ferreira CA, Armelin E, Ferreira JZ, Meneguzzi A. Smart paint for anodic protection of steel. Prog Org Coat. 2015;78:116-23.
- Xue S, Shen R, Chen W, Miao R. Corrosion fatigue failure analysis and service life prediction of high strength steel wire. Eng Fail Anal. 2020;110(104440):1-10.
- [5] Cui C, Chen A, Ma R. An improved continuum damage mechanics model for evaluating corrosion-fatigue life of highstrength steel wires in the real service environment. Int J Fatigue. 2020;135(105540):1-9.
- Lv M, Chen X, Li Z, Du M. Effect of sulfate-reducing bacteria on hydrogen permeation and stress corrosion cracking behavior of 980 high-strength steel in seawater. J Mater Sci Technol. 2021;92:109-19.
- Chen A, Yang Y, Ma R, Li L, Tian H, Pan Z. Experimental study of corrosion effects on high-strength steel wires considering strain influence. Constr Build Mater. 2020;240(117910):1-12.
- Sanchez J, Lee SF, Martin-Rengel MA, Fullea J, Andrade C, Ruiz-Hervías J. Measurement of hydrogen and embrittlement of high strength steels. Eng Fail Anal. 2016;59:467-77.
- Díaz B, Freire L, Nóvoa XR, Pérez MC. Electrochemical behaviour of high strength steel wires in the presence of chlorides. Electrochim Acta. 2009;54(22):5190-8.
- [10] Jain A, Gencturk B, Pirbazari M, Dawood M, Belarbi A, Sohail MG, et al. Influence of pH on chloride binding isotherms

- for cement paste and its components. Cem Concr Res. 2021;143(106378):1-16.
- [11] Mayne JEO, Menter JW. The mechanism of inhibition of the corrosion of iron in sodium hydroxide solution. Part II. J Chem Soc. 1954;99-103.
- [12] Wang X-P, Shao M, Ye C-Q, Dong S-G, Du R-G, Lin C-J. Study on effect of chloride ions on corrosion behavior of reinforcing steel in simulated polluted concrete pore solutions by scanning micro-reference electrode technique. J Electroanal Chem. 2021;895(115454):1-11.
- [13] Lee SF, Jacobsen S. Study of interfacial microstructure, fracture energy, compressive energy and debonding load of steel fiber-reinforced mortar. Mater Struct. 2011;44:1451-65.
- [14] Wang XH, Jacobsen S, He JY, Zhang ZL, Lee SF, Lein HL. Application of nanoindentation testing to study of the interfacial transition zone in steel fiber reinforced mortar. Cem Concr Res. 2009;39:701-15.
- [15] Sáez del Bosque IF, Van den Heede P, De Belie N, Sánchez de Rojas MI, Medina C. Freeze-thaw resistance of concrete containing mixed aggregate and construction and demolition waste-additioned cement in water and de-icing salts. Constr Build Mater. 2020;259(119772):1-15.
- [16] Guo K, Miao H, Liu L, Zhou J, Liu M. Effect of graphene oxide on chloride penetration resistance of recycled concrete. Nanotechnol Rev. 2019;8:681-9.
- Li D, Wei R, Li L, Guan X, Mi X. Pitting corrosion of reinforcing steel bars in chloride contaminated concrete. Constr Build Mater. 2019;199:359-68.
- [18] Liu J-C, Park S, Nagao S, Nogi M, Koga H, Ma J-S, et al. The role of Zn precipitates and Cl⁻ anions in pitting corrosion of Sn-Zn solder alloys. Corros Sci. 2015;92:263-71.
- [19] Chen H, Lu L, Huang Y, Li X. Insight into TiN inclusion induced pit corrosion of interstitial free steel exposed to aerated NaCl solution. J Mater Res Technol. 2021;13:13-24.
- [20] Wang Y, Li MY, Zhu F, Dong WT, Zhang XY, Sun LL. Pitting corrosion mechanism of Cl-- and S2--induced by oxide inclusions in Fe-based amorphous metallic coatings. Surf Coat Technol. 2020;385(125449):1-13.
- [21] Scott GN. Corrosion protection properties of portland cement concrete. I Am Water Work Assoc. 1965:57(8):1038-52.
- [22] Hausmann DA. Steel corrosion in concrete How does it occur. Mater Prot. 1967;19-23.
- [23] Gulbransen EA. Thin oxide films on Iron. Trans Electrochem Soc. 1942;81:327-39.
- [24] Zhang B, San XY, Wei XX, Wu B, Zheng SJ, Zhou YT, et al. Quasi-in-situ observing the growth of native oxide film on the FeCr₁₅Ni₁₅ austenitic alloy by TEM. Corros Sci. 2018;140:1-7.
- Abd El Aal EE, Abd El Wanees S, Diab A, Abd El Haleem SM. [25] Environmental factors affecting the corrosion behavior of reinforcing steel III. Measurement of pitting corrosion currents of steel in Ca(OH)₂ solutions under natural corrosion conditions. Corros Sci. 2009;51(8):1611-8.
- Pourbaix M. Atlas of electrochemical equilibria in aqueous solutions. Houston: Pergamon Press Ltd; 1966.
- Umar A, Ibrahim AA, Kumar R, Albargi H, Alsaiari MA, Ahmed F. Cubic shaped hematite $(\alpha\text{-Fe}_2O_3)$ micro-structures composed of stacked nanosheets for rapid ethanol sensor application. Sens Actuat B-Chem. 2021;326(128851):1-9.
- [28] Tait WS. Chapter 5 Electrochemical corrosion basics. In: Kutz M, editor. Handbook of environmental degradation of

- materials. 3rd edn. New York: William Andrew Applied Science Publishers; 2018. p. 97-115
- [29] Alvarez SM, Bautista A, Velasco F. Corrosion behaviour of corrugated lean duplex stainless steels in simulated concrete pore solutions. Corros Sci. 2011;53(5):1748-55.
- [30] Shi J, Sun W, Jiang J, Zhang Y. Influence of chloride concentration and pre-passivation on the pitting corrosion resistance of low-alloy reinforcing steel in simulated concrete pore solution. Constr Build Mater. 2016;111:805–13.
- [31] Moser RD, Singh PM, Kahn LF, Kurtis KE. Chloride-induced corrosion resistance of high-strength stainless steels in simulated alkaline and carbonated concrete pore solutions. Corros Sci. 2012;57:241–53.
- [32] Hoar TP, Jacob WR. Breakdown of passivity of stainless steel by halide Ions. Nature. 1967;216(5122):1299–301.
- [33] Amin MA, Hassan HH, Abd El Rehim SS. On the role of NO₂⁻ ions in passivity breakdown of Zn in deaerated neutral sodium nitrite solutions and the effect of some inorganic inhibitors potentiodynamic polarization, cyclic voltammetry, SEM and EDX studies. Electrochim Acta. 2008;53:2600–9.
- [34] Bellezze T, Giuliani G, Roventi G. Study of stainless steels corrosion in a strong acid mixture. Part 1: cyclic potentiodynamic polarization curves examined by means of an analytical method. Corros Sci. 2018;130:113-25.
- [35] Ormellese M, Lazzari L, Goidanich S, Fumagalli G, Brenna A. A study of organic substances as inhibitors for chlorideinduced corrosion in concrete. Corros Sci. 2009;51:2959–68.
- [36] Finsgara M, Fassbender S, Hirth S, Milosev I. Electrochemical and XPS study of polyethyleneimines of different molecular sizes as corrosion inhibitors for AISI 430 stainless steel in nearneutral chloride media. Mater Chem Phys. 2009;116:198–206.
- [37] Yuan X, Wang X, Cao Y, Yang H. Natural passivation behavior and its influence on chloride-induced corrosion resistance of stainless steel in simulated concrete pore solution. J Mater Res Technol. 2020;9(6):12378-90.
- [38] Liu M, Cheng X, Li X, Zhou C, Tan H. Effect of carbonation on the electrochemical behavior of corrosion resistance low alloy steel rebars in cement extract solution. Constr Build Mater. 2017:130:193–201.
- [39] Zhong L, Xiao S, Hu J, Zhu H, Gan F. Application of polyaniline to galvanic anodic protection on stainless steel in H₂SO₄ solutions. Corros Sci. 2006;48:3960-8.
- [40] Wang Y, Cheng G, Wu W, Qiao Q, Li Y, Li X. Effect of pH and chloride on the micro-mechanism of pitting corrosion for high strength pipeline steel in aerated NaCl solutions. Appl Surf Sci. 2015;349:746–56.
- [41] Mohammed S, Hua Y, Barker R, Neville A. Investigating pitting in X65 carbon steel using potentiostatic polarisation. Appl Surf Sci. 2017;423:25–32.

- [42] Zhang S, Li Y, Wei Y, Liu B, Du H, Wei H, et al. Synergistic effect of chloride ions and filmed surface on pitting in the pseudopassivation behavior of carbon steel. Vacuum. 2021;185(110042):1-4.
- [43] Dong F, Venezuela J, Li H, Shi Z, Zhou Q, Chen L, et al. Effect of vanadium and rare earth microalloying on the hydrogen embrittlement susceptibility of a Fe-18Mn-0.6C TWIP steel studied using the linearly increasing stress test. Corros Sci. 2021;185(109440):1–17.
- [44] Kim K-S, Kang J-H, Kim S-J. Carbon effect on hydrogen diffusivity and embrittlement in austenitic stainless steels. Corros Sci. 2021;180(109226):1–9.
- [45] Dong ZH, Shi W, Guo XP. Initiation and repassivation of pitting corrosion of carbon steel in carbonated concrete pore solution. Corros Sci. 2011;53:1322-30.
- [46] Semino CJ, Galvele JR. Passivity breakdown of high purity iron and AISI 4340 steel in 0.5M NaCl solution. Corros Sci. 1976;16(5):297–306.
- [47] Ya V, Martin N, Chou Y-H, Chen Y-M, Choo K-H, Chen S-S, et al. Electrochemical treatment for simultaneous removal of heavy metals and organics from surface finishing wastewater using sacrificial iron anode. J Taiwan Inst Chem Eng. 2018:83:107–14.
- [48] Huang Y, Liu X, Zhang Q, Xu Y, Kunte H-J, De, et al. Hydrogen release from carbon steel in chloride solution under anodic polarization. Int J Hydrog Energy. 2020;45:3307–15.
- [49] Targhoo A, Amiri A, Baghayeri M. Magnetic nanoparticles coated with poly(p-phenylenediamine-co-thiophene) as a sorbent for preconcentration of organophosphorus pesticides. Microchim Acta. 2018;185(15):1–8.
- [50] Mahdavi M, Bin Ahmad M, Haron MJ, Namvar F, Nadi B, Rahman MZA, et al. Synthesis, surface modification and characterisation of biocompatible magnetic iron oxide nanoparticles for biomedical applications. Molecules. 2013;18:7533-48.
- [51] Ma P, Luo Q, Chen J, Gan Y, Du J, Ding S, et al. Intraperitoneal injection of magnetic Fe₃O₄-nanoparticle induces hepatic and renal tissue injury via oxidative stress in mice. Int J Nanomed. 2012;7:4809-18.
- [52] Chougale UM, Fulari VJ. Facile synthesis of maghemite nanoflakes arrays for supercapacitor application. Mater Sci Semicond Process. 2014;27:682–8.
- [53] Shi J, Li M, Wu M, Ming J. Role of red mud in natural passivation and chloride-induced depassivation of reinforcing steels in alkaline concrete pore solutions. Corros Sci. 2021;190(109669):1–16.
- [54] Galvele JR. Transport Processes and mechanism of pitting of metals. J Electrochem Soc. 1976;123(4):464-74.